RSC Advances

ROYAL SOCIETY OF CHEMISTRY

www.rsc.org/advances

RSC Advances

ARTICLE

Received 00th January 20xx,

Accepted 00th January 20xx

DOI: 10.1039/x0xx00000x

www.rsc.org/

Blue-Silica by Eu^{2+}-Activator Occupied in Interstitial Sites

Donghyeon Kim,[a] Yoeng-Hun Jin,[b] Ki-Wan Jeon,[c] Sungyun Kim,[d] Seung-Joo Kim,[e] Oc Hee Han,[f] Dong-Kyun Seo[c] and Jung-Chul Park[*ab]

Blue-emitting $SiO_2:Eu^{2+}$ compound has been successfully synthesized and characterized. The PL intensity of $SiO_2:Eu^{2+}_{0.002}$ compound is about 24 times higher than that of the O-defective SiO_2 compound (without activators) which emits blue light. The valence state of Eu ions as the nature of the highly enhanced blue emission in resulting material, is determined to be Eu^{2+} using reference materials ($EuCl_2$ and $EuCl_3$) in XPS measurements. The Eu^{2+}-activator ions occupied in the interstitial sites of SiO_2 matrix, are confirmed by FT-IR, XPS, and ^{29}Si MAS-NMR spectroscopy. Even though the void spaces formed structurally in both α-quartz and α-cristobalite can accommodate Eu^{2+} ions (ionic radius = 1.25 Å at CN = 8), $SiO_2:Eu^{2+}$ compound fired at 1300℃ under hydrogen atmosphere is destined to be deficient in O or Si atoms, indicating the formation of the wider void spaces in SiO_2 crystal lattice. A sputtered depth profile of SiO_2-related compounds obtained by time-of-flight secondary ion mass spectrometry (TOF-SIMS) corroborates the O-defective SiO_2 induced by hydrogen. In particular, the interatomic potentials depending on the interstitial positions of Eu atom in α-cristobalite and α-quartz are calculated based on Lennard-Jones potential and coulomb potential; for α-cristobalite the minimum potential value is -51.47 eV, for α-quartz 221.8 eV, which reveals that the Eu^{2+}-activator ions more preferably enter the interstitial sites of α-cristobalite than those of α-quartz. Thanks to the stable Eu^{2+}-activator ions enclosed by Si-O linkages, $SiO_2:Eu^{2+}_{0.002}$ compound emits blue light and its PL emission intensity is about 24 times higher than that of the O-defective SiO_2 compound. This phosphor material could be a platform for modeling a new phosphor and application in the solid-state lighting field.

1 Introduction

Silicone (27.2 wt %) is the most abundant element in the earth's crust after oxygen (45.5 %), and silicone never occurs free but invariably occurs combined with 4-coordinated oxygen in nature. The [SiO_4] unit may occur as an individual group or be linked into chains, ribbons, sheets, or three-dimensional frameworks.[1] Silica, or silicon dioxide (SiO_2) naturally occurs in both crystalline and amorphous forms. The various forms of the crystalline silica are: α-quartz, β-quartz, α-tridymite, β-tridymite, α-cristobalite, β-cristobalite, keatite, coesite, stishovite, and moganite.[2] The most abundant form of the silica is α-quartz which is the most thermodynamically stable form of the crystalline silica in ambient conditions. Quartz has been used for a long time (several thousand years) in jewelry as a gem stone, and is used extensively in electronics as well as optical components industries.[3] It is very interesting that Zolensky et al. reported that blue quartz phenocrysts from the Llano rhyolite (Ilanite), Llano County, and Texas, derived their coloration from Rayleigh scattering by abundant submicrometer-sized ilmenite inclusions, without experimental evidences.[4] According to their results, the concentrations of rare-earth element (REE) in the blue quartz were determined as 0.910 ppm (Ce), 0.108 ppm (Sm), 0.016 ppm (Eu), 0.029 ppm (Tb), 0.332 ppm (Yb), and 0.064 ppm (Lu). It is well-known that in phosphor materials various activators, such as Nd^{3+}, Pr^{3+}, Sm^{3+}, Eu^{3+}, Eu^{2+}, Ce^{3+}, Tb^{3+}, Yb^{3+} etc., have been widely used for flat panel displays and optoelectronic devices.[5-8] Among them, the divalent europium ions (Eu^{2+}) have been considered as a very important and useful activator which exhibits broad emission bands between ultraviolet (UV) and red spectral range associated with $4f^65d^1$ - $4f^7$ transition.[9-11] Considering various activator ions, it is presumed that the origin of blue coloration in quartz from the Llano rhyolite (Ilanite), Llano County, and Texas, may be due to the Eu^{2+} or Ce^{3+} ions occupied into the crystal lattice of quartz. Zolensky et al., however, argued that the blue quartz is originated from

[a] Graduate School of Advanced Engineering, Silla University, Busan 617-736, Republic of Korea. E-mail: parkjc@silla.ac.kr
[b] Center for Green Fusion Technology and Department of Engineering in Energy & Applied Chemistry, Silla University, Busan617-736, Republic of Korea
[c] Department of Chemistry and Biochemistry, Arizona State University, Tempe, AZ 85287-1604, USA
[d] Institute of NT.IT Fusion Technology, Energy Center 401, Ajou University, Suwon 443-749, Republic of Korea.
[e] Department of Chemistry, Division of Energy Systems Research, Ajou University, Suwon 443-749, Republic of Korea
[f] Western Seoul Center, Korea Basic Science Institute University-Industry Cooperation Building 150 Bukahyun-ro, Seodaemun-gu, Seoul 120-140, and Graduate School of Analytical Science & Technology Chungnam National University, Daejeon 305-764, Republic of Korea

Rayleigh scattering by the ilmenite inclusions because the large difference in the ionic radii of Si^{4+} (0.40 Å) and Eu^{2+} (1.31 Å) precludes direct substitution.[4] It is very interesting that the blue emission induced by the O-related defects (without activator ions) in SiO_2-related compounds, was reported by several groups.[12-18] Uchino et al. proposed that the blue-emitting center in oxidized porous silicone and nano-SiO_2 materials, is a metastable defect pair consisting of =Si(O_2) and =Si:, on the basis of the density functional theory calculation, which was in good agreement with the peak positions of the PLE from the blue-emitting materials.[14] McCrate et al. also presented that the intrinsic oxygen vacancy defect (OVD) on planar fused silica was experimentally detected by titration with fluorescent probe molecules, such as perylene-3-methanamine and 3-vinyl perylene.[18] Blue emission by Ce^{3+} ions occupied in the interstitial site of AlN structure was reported by Liu et al.[19] According to their results, an octahedral interstitial site of the AlN compound with würtzite structure was proposed to be the site for Ce^{3+} ions because the ionic size of Ce^{3+} ions is much larger than that of Al^{3+}. It should be noted that there is an interstitial sites formed structurally in the crystal lattice of α-quartz (or. α-cristobalite) and possibilities for Ce^{3+} or Eu^{2+} activator ions to enter the interstitial sites of α-quartz (or. α-cristobalite), which probably results in the blue coloration in α-quartz (or. α-cristobalite). In this work, we report synthesis and characterization of a blue silica induced by Eu^{2+}-activator ions occupied in interstitial sites. In particular, the Eu^{2+}-doping mechanism in SiO_2 matrix is discussed using Photoluminescence (PL) apparatus, Rietveld refinements, Nano-Secondary Ion Mass Spectrometry (Nano-SIMS), X-ray photoelectron spectroscopy (XPS), ^{29}Si magic-angle-spinning nuclear magnetic resonance (MAS-NMR) spectrometer, and theoretical calculation of the interatomic potential based on Lennard-Jones potential and coulomb potential.

2 Experimental

The polycrystalline SiO_2:Eu compounds have been prepared from a mixture of SiO_2 (quartz) and Eu_2O_3 using NH_4Cl as a flux and lubricant under 4% H_2-Ar mixture gas between 1000℃ and 1500℃ for 6 h. Alumina boats covered with lid were used in order to maximize collision time among starting materials (SiO_2, NH_4Cl, and Eu_2O_3), and to prevent loss of unreacted NH_4Cl from a rapid out-gassing. In the firing step, each mixture was initially heated at 450℃ for 1 h, and subsequently heated at final temperature for 3 h (heating rate : 3℃ min^{-1}). Powder X-ray diffraction measurements of SiO_2:Eu were carried out using a X-ray diffractometer equipped with a graphite monochromator (DMAX-2200PC, Rigaku). A step scan mode was employed in a 2ϑ range 10–110° with a step size of 0.02° and counting time of five second for each step. Structure refinements were carried out by the Rietveld method using the Fullprof program[20] with pseudo-Voïgt peak shapes and refined backgrounds. The photoluminescence (PL) spectra were obtained at room temperature using a fluorescent spectrophotometer with a 150 W Xenon lamp under an operating voltage of 350 V (Fluorometer FS-2, Scinco). The reflectance spectra were recorded using UV-visible spectrophotometer (UV-2600, Shimadzu) with $BaSO_4$ as a reference. Fourier-transform infrared spectroscopy (FT-IR) was performed using a FT-IR spectrophotometer (IRTracer-100, Shimadzu) with the resolution range of ± 0.5 cm^{-1} and a KBr medium prepared with 0.5 wt% of sample. The Nano-Secondary Ion Mass Spectrometry (NanoSIMS) measurements were done using a rastering Cs^+ primary ion beam on the Cameca Ametek NanoSIMS 50L at Arizona State University. The beam current at the sample was lowered to ~0.48 pA by choosing a small diaphragm to obtain fine beam. Although the low current used for analysis, the new capillary Cs source produced a high primary beam density and high secondary ion count rates during imaging. Negative secondary ions of $^{24}Si^-$ and $^{16}O^-$ were measured simultaneously using electron multipliers in the multi-collection mode. The measurement of NanoSIMS for all samples was performed after pre-sputtering for 5 min. All samples for NanoSIMS measurement were prepared by the following: 500 mg of sample was dispersed in 5 mL of the absolute ethanol by ultrasound sonication for 10 min. The obtained milky suspension after sonication was dripped by pipet on stainless-steel substrate (1-cm diameter) and dried at ambient conditions. This was repeated until white thick coating was obtained on the substrate. The oxidation states of the elements were analyzed by X-ray photoelectron spectroscopy (XPS, ESCALAB 250) with a monochromatic Al K_α X-ray source (hv = 1486.6 eV) at Busan Center of Korea Basic Science Institute (KBSI). The obtained binding energies (BEs) were calibrated with that of adventitious carbon (C 1s) core level peak at 284.6 eV as a reference. All ^{29}Si single-pulse magic angle spinning (SP MAS) spectra were acquired using a Unity INOVA 600 MHz NMR instrument (Agilent Technologies, U. S. A.) with a cross polarization (CP) MAS probe for 5 mm Zirconia rotors at room temperature, a 30° pulse corresponding to 2 μs, a pulse repetition delay of 20 s, a spectral width of 120 kHz, and a spinning rate of 10 kHz. The chemical shifts were referenced to external tetramethylsilane at 0 ppm.

3 Results and discussion

3.1 Structural Characterization

Structure refinements of the samples were carried out using a Rietveld program. The background was fitted with a polynomial function and the peak shape was modelled using a pseudo-Voïgt function. The observed, calculated, and difference patterns from the Rietveld refinements of the X-ray diffraction data are shown in Fig. 1. The profile of undoped SiO_2 fired at 1300℃ under 4% H_2-Ar atmosphere contains α-cristobalite as major phase (90%) and quartz as second phase (10%). The atomic coordinates of the both structures were initially selected from data base (α-cristobalite: ICSD # 75300, α-quartz: ICSD # 647436). The relative proportion of phases, final structural parameters (lattice parameters, refined atomic positions, and isotropic temperature factors for all atoms) and reliability factors are listed in Table 1. In comparison with the

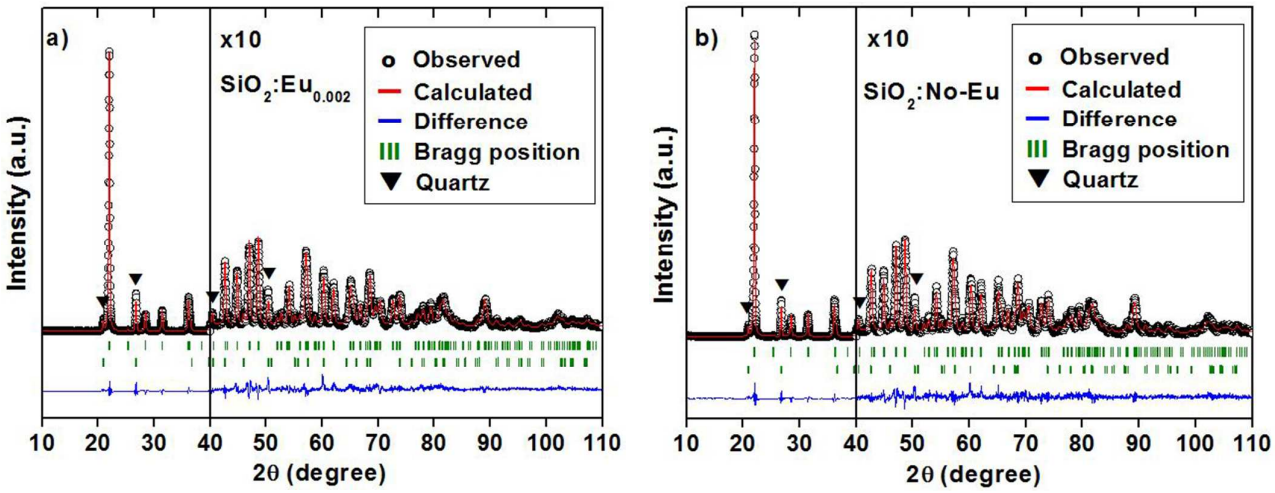

Fig. 1 Rietveld refinement of the powder XRD profiles for SiO_2:$Eu_{0.002}$ (a) and undoped SiO_2 (b). The diffraction pattern is composed of the peaks from α-cristobalite as a main phase and α-quartz as a minor phase. Measured data, fitted results, expected reflection positions, and the difference between measured and fitted results are expressed as red open circles, black solid lines, black vertical lines, and blue solid lines, respectively. The peak intensities over 40 degrees in 2θ have been magnified 10 times for clarity.

Table 1 Relative Proportion of Phases, Structural Parameters and Reliability Factors for SiO_2:$Eu_{0.002}$ and SiO_2

Compound		**SiO_2:$Eu_{0.002}$**		**SiO_2:No-Eu**	
Phase		**α-Cristobalite**	**α-Quartz**	**α-Cristobalite**	**α-Quartz**
Weight present (%)		89.2(4)	10.8(13)	90.1(5)	9.9(17)
R_{wp} (%)		11.1		13.0	
R_{bragg}		2.63	7.60	2.89	6.69
R_f (%)		2.98	4.53	3.17	4.61
χ^2		1.51		2.12	
Space group		$P4_12_12$ (No. 92)	$P3_221$ (No. 154)	$P4_12_12$ (No. 92)	$P3_221$ (No. 154)
Lattice Parameter (Å)	a	4.9768(2)	4.9030(5)	4.9732(3)	4.9041(6)
	c	6.9490(4)	5.3831(8)	6.9362(4)	5.3851(9)
Cell volume (Å^3)		172.12(14)	112.07(3)	171.55(16)	112.16(3)

Compound	**SiO_2:$Eu_{0.002}$ (α-Cristobalite)**	**SiO_2:No-Eu (α-Cristobalite)**	**SiO_2:$Eu_{0.002}$ (α-Quartz)**	**SiO_2:No-Eu (α-Quartz)**
Si, 4a			Si, 3a	
x	0.2967(2)	0.2966(2)	x	0.470(2)	0.469(2)
y	0.2967(2)	0.2966(2)	y	0	0
z	0	0	z	2/3	2/3
Site occupancies	1	1	Site occupancies	1	1
B_{iso} (Å^2)	1.39(3)	1.18(3)	B_{iso} (Å^2)	0.5(1)	0.4(1)
O, 8b			O, 6c		
x	0.2412(4)	0.2428(5)	x	0.439(2)	0.433(2)
y	0.0985(4)	0.1012(5)	y	0.279(2)	0.276(2)
z	0.1756(3)	0.1757(3)	z	0.786(2)	0.783(2)
Site occupancies	1	1	Site occupancies	1	1
B_{iso} (Å^2)	1.78(6)	1.36(6)	B_{iso} (Å^2)	2.1(3)	1.7(4)

Table 2 Unit Cell Parameters and Phase Content between α-Quartz and α-Cristobalite in Silicas Fired under 4% H_2-Ar Atmosphere

Compound	α-Cristobalite (weight %)	a (Å)	c (Å)	α-Quartz (weight %)	a (Å)	c (Å)
SiO_2 (Aldrich chemical)	-	-	-	100%	4.91202(13)	5.40345(17)
SiO_2 (1500℃)	100%	4.97114(19)	6.9254(3)	-	-	-
SiO_2 (1300℃)	90.03%	4.9731(3)	6.9362(4)	9.97%	4.9043(6)	5.3844(10)
SiO_2:$Eu_{0.002}$ (1300℃)	89.20%	4.9767(2)	6.9491(4)	10.80%	4.9035(6)	5.38214
SiO_2:$Eu_{0.05}$ (1300℃)	99.07%	4.9733(2)	6.9341(3)	0.93%	4.90(5)	5.38(9)

undoped SiO_2, the Eu-doped SiO_2 compound showed no substantial difference in the crystal structure except for the temperature factors. For instance, the isotropic temperature factors, B_{iso} of Si and O atoms are 1.18(3) $Å^2$ and 1.36(6) $Å^2$ for the α-cristobalite phase in undoped SiO_2, while those are 1.39(3) $Å^2$ and 1.78(6) $Å^2$ in doped SiO_2:$Eu_{0.002}$. The large temperature factors for SiO_2: $Eu_{0.002}$ imply that the Eu doping into SiO_2 leads to the increase of structural disorder. Table 2 shows the weight percentages (%) of α-quartz and α-cristobalite as a function of firing temperature and Eu content. It is evident that the weight % of α-cristobalite is increased with increasing firing temperature and Eu content.

3.2 Photoluminescence Spectra

Fig. 2 presents the PL spectra of SiO_2:$Eu_{0.01}$ synthesized under 4 % H_2-Ar atmosphere as a function of firing temperature. The highest excitation and emission intensity are observed in the SiO_2:$Eu_{0.01}$ compound synthesized at 1300℃ that is an optimal firing temperature. The excitation spectra of SiO_2:$Eu_{0.01}$ compounds monitored at 438 nm, consist of broad bands between 220 nm and 420 nm, which may be ascribed to the allowed $4f^7 - 4f^6 5d$ transitions of Eu^{2+}.[21-23] The emission spectra

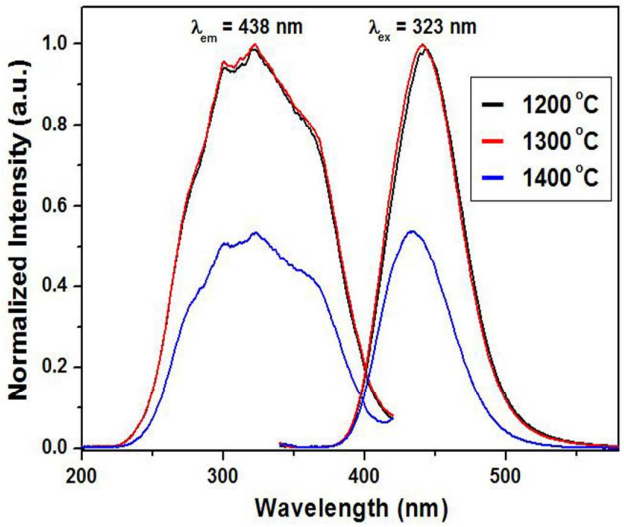

Fig. 2 Excitation and emission spectra of SiO2:Eu0.01 as a function of firing temperature.

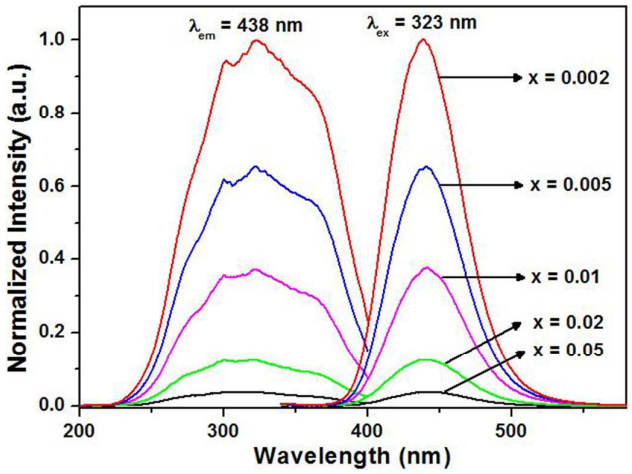

Fig. 3 Excitation and emission spectra of SiO_2: Eu_x^{2+} as a function of Eu content.

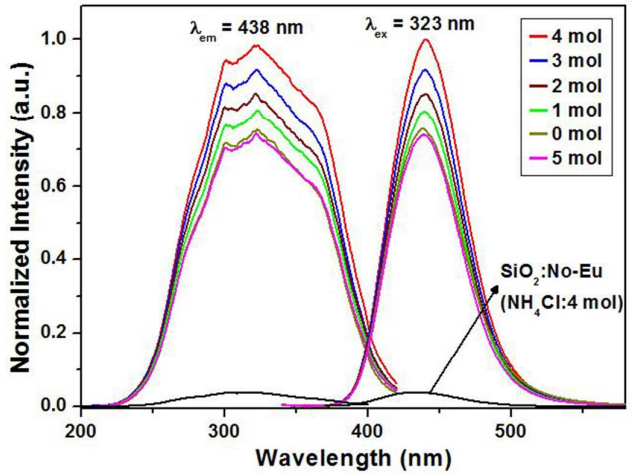

Fig. 4 Excitation and emission spectra of SiO_2: $Eu_{0.002}^{2+}$ as a function of NH_4Cl mole.

monitored under the 323 nm excitation, show symmetric bands centered around 438 nm, which is associated with blue-emission. The excitation and emission spectra of SiO_2:Eu_x compounds synthesized at 1300℃ as a function of Eu content are shown in Fig. 3. The PL maximum intensity is observed at x = 0.002, then decreased with increasing Eu concentration. The optimum concentration of Eu in the SiO_2:Eu compound is

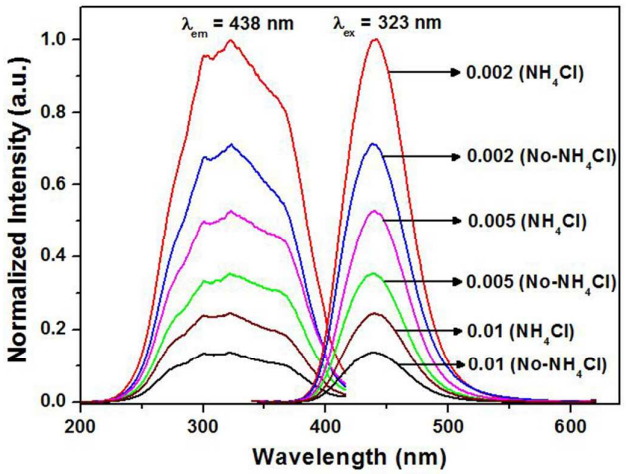

Fig. 5 Excitation and emission spectra of SiO_2: Eu_x^{2+} with and without NH_4Cl (4 moles).

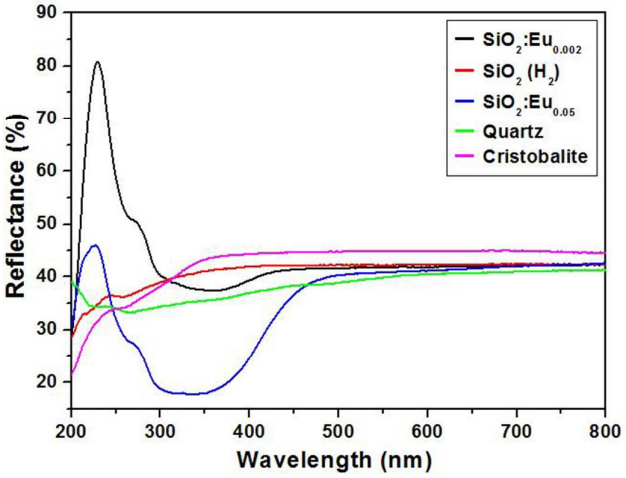

Fig. 6 Diffuse reflectance spectra of SiO_2-related compounds.

0.002, which implies that SiO_2 crystal lattice is difficult to accommodate the large amount of Eu^{2+}-activator ions. It should be noted that NH_4Cl is widely used as a flux and lubricant chemical in solid-state reaction because of a ralatively low melting point (340℃) and boiling point (520℃). In this work, NH_4Cl plays an important role in SiO_2:Eu compounds as a flux and lubricant which forces Eu^{2+} to enter the interstitial sites of SiO_2 matrix. As shown in Fig. 4, the PL intensity of $SiO_2:Eu_{0.002}^{2+}$ is increased With the higher mole ratio between NH_4Cl and SiO_2 (mole(NH_4Cl)/mole(SiO_2)). The maximum PL intensity is observed at the mole ratio 4. It is very noteworthy that the PL pattern of SiO_2 (No-Eu, 4 mole NH_4Cl) is similar to that of $SiO_2:Eu_{0.002}^{2+}$ except the difference of the PL intensities, indicating the blue emissions induced by the O-related defects (without activator ions) in SiO_2-related compounds[12-18] as mentioned in introduction. It is very remarkable that the PL intensity of $SiO_2:Eu_{0.002}^{2+}$ is about 24 times as high as that of SiO_2 (No-Eu, 4 mole NH_4Cl) fired at

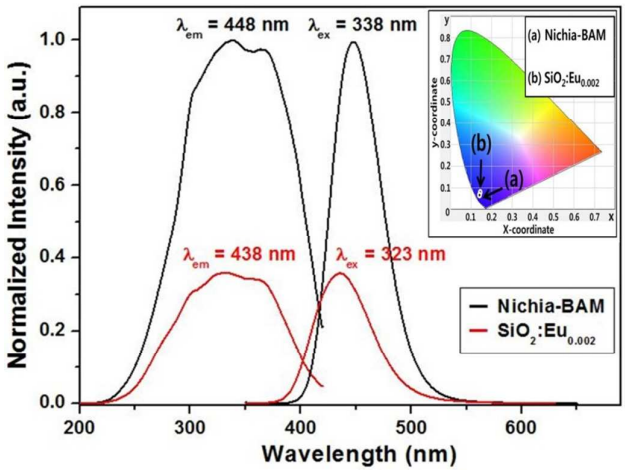

Fig. 7 PL spectra of $SiO_2:Eu_{0.002}^{2+}$ and a commercial $BaMgAl_{10}O_{17}:Eu^{2+}$ (BAM) phosphor (obtained from Nichia corp., Japan). The inset shows the CIE chromaticity for two phosphors depending on the excitation UV light.

1300℃ under 4% H_2-Ar atmosphere, which is probably due to the Eu ions occupied into the SiO_2 matrix. Fig. 5 presents the PL spectra of $SiO_2:Eu_x^{2+}$ (x = 0.002, 0.005, and 0.010) with and without NH_4Cl addition. For SiO_2: $Eu_{0.002}^{2+}$ compound, it prominently shows that the emission intensity (at 438 nm) of the resulting materials after NH_4Cl addition is 1.4 times higher than that of the resulting materials without NH_4Cl addition. This result implies that NH_4Cl shows a considerable effect on the PL intensity and plays an important role as a flux and lubricant in $SiO_2:Eu_x^{2+}$compounds. Fig. 6 presents the diffuse reflectance spectra of SiO_2 and $SiO_2:Eu_x^{2+}$ (x = 0.002 and 0.05). When Eu^{2+} ions are occupied into the SiO_2 matrix, the broad absorption bands are shown between 220 nm and 450 nm, whereas absorption bands are not shown in α-quartz and α-cristobalite in the region. It might indicate the broad absorption bands between 220 nm and 450 nm are associated with the 4f→5d transition of Eu^{2+}. Also, the absorption bands of $SiO_2:Eu_{0.002}^{2+}$ are still stronger than that of $SiO_2:Eu_{0.05}^{2+}$, which is well consistent with PL results as previously shown in Fig. 3. The luminescent behavior of $SiO_2:Eu_{0.002}^{2+}$ compound synthesized at 1300℃ under 4% H_2-Ar atmosphere with the mole ratio = 4 (mole (NH_4Cl)/mole (SiO_2)) was compared with a commercial $BaMgAl_{10}O_{17}:Eu^{2+}$ (BAM:Eu^{2+}) phosphor (obtained from Nichia corp., Japan). The excitation and emission spectra of $SiO_2:Eu_{0.002}^{2+}$ and BAM:Eu^{2+} phosphor are shown in Fig. 7. The excitation and emission spectra are very similar except the difference in the PL intensity. The relative emission intensity of $SiO_2:Eu_{0.002}^{2+}$ monitored at 323 nm is about 40% compared to a commercial BAM:Eu^{2+}. The Commission International de l'Eclairage (CIE) coordinates of $SiO_2:Eu_{0.002}^{2+}$ and BAM:Eu^{2+} monitored under UV light at 300 nm, are x = 0.145, y = 0.068 and x = 0.143, y = 0.065, respectively as shown in the inset of Fig. 7. According to CIE coordinates, it directly indicates that the $SiO_2:Eu_{0.002}^{2+}$ compound emits deep blue.

3.3 Infrared Spectroscopy

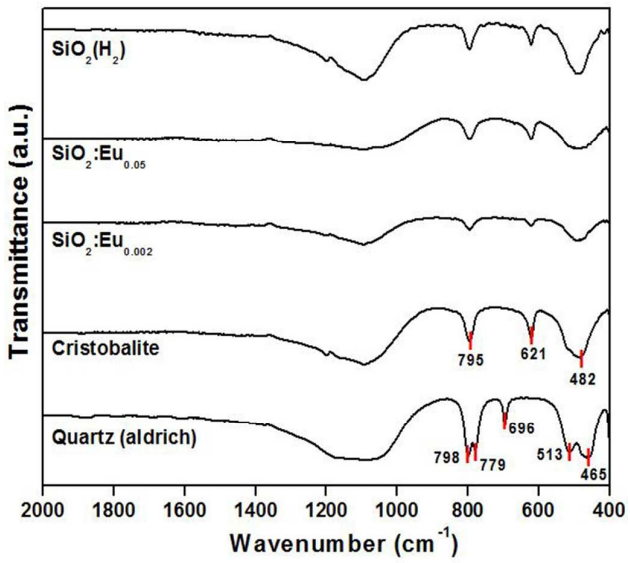

Fig. 8 Infrared spectra of SiO_2-related compounds.

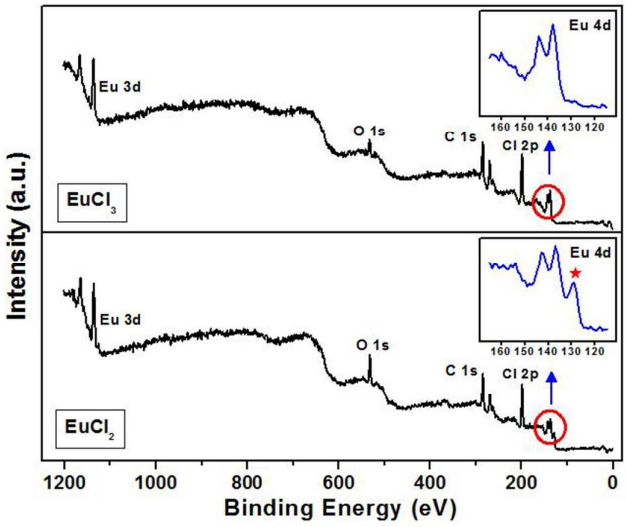

Fig. 9 Wide scan XPS spectra of reference compounds, $EuCl_2$ and $EuCl_3$.

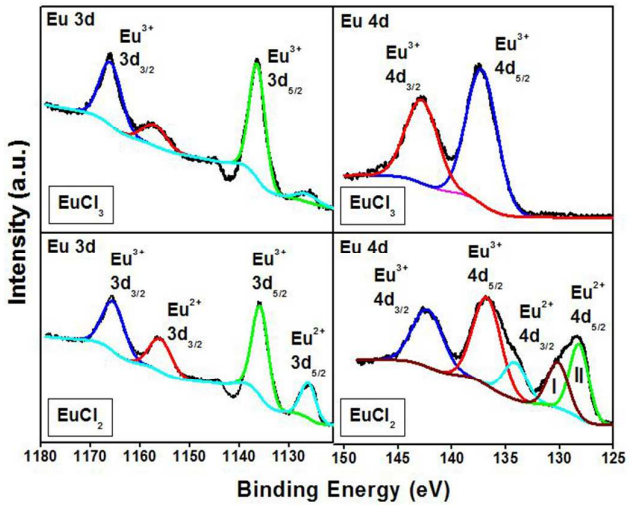

Fig. 10 High-resolution Eu 3d and 4d XPS spectra of reference compounds, $EuCl_2$ and $EuCl_3$.

Fig. 8 presents the IR spectra of SiO_2-related compounds. The absorption band at 1092 cm^{-1} in the spectra of α-quartz is associated with Si–O asymmetrical stretching vibrations, those at 799 and 780 cm^{-1} with Si–O symmetrical stretching vibrations, that at 696 cm^{-1} with Si–O symmetrical bending vibrations, and those at 512 and 460 cm^{-1} with Si–O asymmetrical bending vibrations.[24] After firing α-quartz at 1500°C, the IR spectrum of α-quartz is completely transformed into that of α-cristobalite with a notable new band at 621 cm^{-1} corresponding to Si–O asymmetrical bending vibrations.[25] In SiO_2:Eu^{2+} compounds fired at 1300℃ under 4% H_2-Ar atmosphere, there is no considerable wavenumber shift in IR modes except that the lower absorbance and greater broadness of IR modes compared with those of α-cristobalite. The IR modes in SiO_2 compound (without Eu) fired at 1300°C under 4% H_2-Ar atmosphere, reveals that the Eu ions occupied in SiO_2 matrix might have an effect on the SiO_2 internal modes. As a consequence of the interaction, (Eu^{2+}···[O-Si-O]$^{4-}$···Eu^{2+}), the local symmetry of SiO_2 matrix may be partially collapsed, which results in the modification of the [SiO_4] internal modes, i.e., the lower absorbance and greater broadness of IR modes because there is not enough Eu content to induce the chemical shift of the vibration modes of SiO_2:Eu compounds.[26] It should be noted that the variation of the IR modes by Eu ion doped in SiO_2 matrix means that there is a pseudo-covalent bond character between Eu ion and O ion sharing with SiO_4 tetrahedral units. Thus, it might indicate that Eu ions are occupied in the SiO_2 interstitial sites formed structurally, particularly, in wider ones formed under 4% H_2-Ar atmosphere.

3.4 X-ray Photoelectron and Solid NMR Spectroscopy

In order to examine the valence state of Eu ions occupied into the SiO_2 matrix, XPS analysis was performed. All the XPS spectra were fitted after a Shirley background correction. Fig. 9 presents the wide-scan XPS spectra of $EuCl_2$ (Eu^{2+}) and $EuCl_3$ (Eu^{3+}) reference compounds. It should be pointed out that it is very difficult to obtain fully reduced Eu^{2+} in metal oxide-phosphor compounds based on the standard reduction potential (Eu^{3+}/Eu^{2+} = -0.36 V *vs.* standard hydrogen electrode (SHE)),[27] which indicates that the reduction of Eu^{3+} to Eu^{2+} requires an annealing process at high temperature (≥1000℃) under a reducing atmosphere, such as H_2 or H_2-Ar mixture gas. Additionally, the thermodynamically unstable Eu^{2+} ions are prone to be easily oxidized by foreign molecules, such as H_2O, O_2 etc., in particular, under X-ray irradiation in XPS measurements. As shown in the inset of Fig. 9, the fact that the new band around 128 eV is observed in $EuCl_2$ compound, supports the partial oxidation of Eu^{2+} to Eu^{3+}. Fig. 10 presents

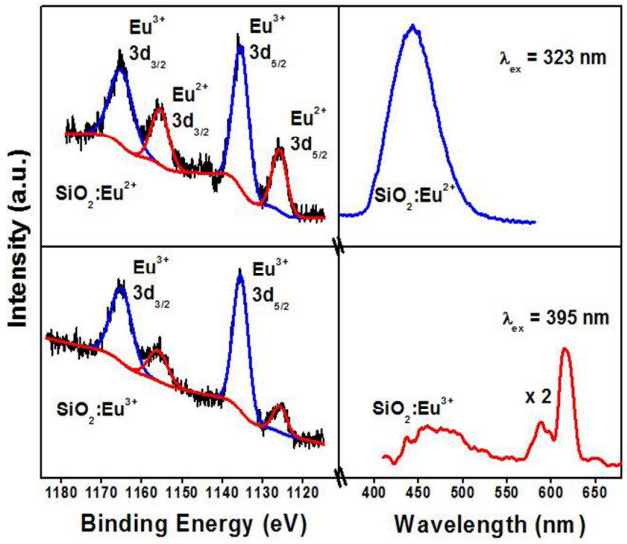

Fig. 11 High-resolution Eu 3d XPS spectra and PL emission spectra of SiO_2:$Eu^{2+}_{0.05}$ and SiO_2:$Eu^{3+}_{0.05}$.

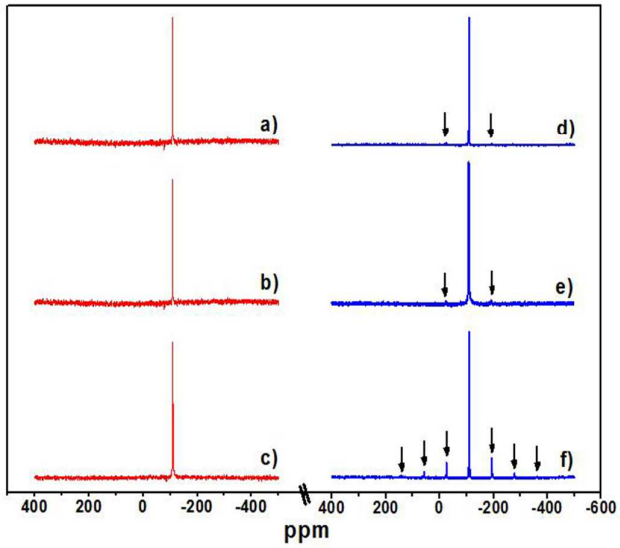

Fig. 12 ^{29}Si MAS-NMR spectra of SiO_2-related compounds; (a) α-quartz, (b) α-cristobalite after firing α-quartz at 1500℃ under H_2, (c) SiO_2 fired at 1300℃ under H_2, (d) SiO_2:$Eu^{2+}_{0.002}$ fired at 1500℃ under H_2, (e) SiO_2:$Eu^{2+}_{0.002}$ fired at 1300℃ under H_2, and (f) SiO_2:$Eu^{2+}_{0.05}$ fired at 1300℃ under H_2. The spinning side-bands are marked by arrows.

Eu 3d and Eu 4d XPS spectra of $EuCl_2$ and $EuCl_3$. The Eu 4d binding energies of $EuCl_3$ (top at right) are assigned to the Eu^{3+} $4d_{5/2}$ (137.3 eV) and Eu^{3+} $4d_{3/2}$ (142.9 eV).[28-30] The spin-orbital splitting value for Eu^{3+} ion is 5.6 eV, which is in good agreement with that as previously reported.[28] The Eu 4d binding energies of $EuCl_2$ (bottom at right) are assigned to Eu^{2+} $4d_{5/2}$ (128.4 eV), Eu^{2+} $4d_{3/2}$ (134.2 eV), Eu^{3+} $4d_{5/2}$ (136.7 eV), and Eu^{3+} $4d_{3/2}$ (142.3 eV), which is well consistent with XPS results as previously reported.[31-36] Notably, Jiang et al. synthesized $EuCl_2$ nanoprisms and nanorods and presented Eu 4d XPS spectra, as follows:[36] Eu^{2+} $4d_{5/2}$ (128.2 eV), Eu^{2+} $4d_{3/2}$ (~134 eV), Eu^{3+} $4d_{5/2}$ (~136 eV), and Eu^{3+} $4d_{3/2}$ (142.2 eV), which is in good agreement with our result. They mentioned, additionally, that Eu 4d XPS spectrum showed the clear presence of Eu^{2+} (128.2 eV and ~134 eV) although the Eu^{2+} ions on the surface were oxidized to Eu^{3+} (~136 eV and 142.2 eV). As shown in Fig. 10 (bottom at right), the spin-orbital splitting values of Eu^{3+} and Eu^{2+} ion (for $EuCl_2$) are 5.6 eV and 5.8 eV, respectively. Interestingly, the Eu^{2+} $4d_{5/2}$ peak at 128.4 eV consists of two components with the spin-orbit splitting value of 5.8 eV, which may be attributed to the different sites of the Eu^{2+} $4d_{5/2}$ induced by the partial oxidation of Eu^{2+}. From the XPS measurement for $EuCl_2$ and $EuCl_3$ reference compounds, it clearly shows that $EuCl_2$ (Eu^{2+}) compound is more sensitive than $EuCl_3$ (Eu^{3+}) in oxidation induced by X-ray irradiation. By the aid of the Eu 4d binding energy for $EuCl_2$ and $EuCl_3$ reference compounds, the XPS 3d binding energies of reference compounds could be precisely assigned as presented in Fig. 10. The Eu 3d binding energies of $EuCl_3$ reference compound (top at left) are assigned to the Eu^{3+} $3d_{5/2}$ (1136.5eV) and Eu^{3+} $3d_{3/2}$ (1166.1 eV) with the small amount of Eu^{2+} state at lower binding energy. On the other hand, the peaks of the Eu^{2+} 3d binding energies for $EuCl_2$ reference compound (bottom at left) are strongly intensified compared with those of $EuCl_3$ compound, i.e., Eu^{2+} $3d_{5/2}$ (1126.3 eV) and Eu^{2+} $3d_{3/2}$ (1156.2 eV). In particular, it is reasonable that the Eu^{2+} valence state in $EuCl_2$ compound is prone to be easily oxidized under X-ray irradiation as presented in Eu 3d as well as Eu 4d XPS spectra. It should be noted that the difference in 3d binding energies between Eu^{2+} and Eu^{3+} (9.7 eV) is somewhat larger than that in 4d binding energies (8.3 eV). It is reasonable considering that the 3d electrons are closer to the nucleus than the 4d elections and thus their binding energies are more strongly affected ($\Delta B.E \propto 1/r$). In order to examine the valence state of Eu ions occupied into the interstitial sites of SiO_2, XPS measurements were performed and its results were presented in Fig. 11. As the PL spectrum (top at right) of SiO_2:$Eu^{2+}_{0.05}$ compound synthesized under 5% H_2-Ar mixture gas, shows the characteristic of Eu^{2+}, $4f^6 5d \rightarrow 4f^7$ transition with a broad band between 380 nm and 520 nm corresponds to the blue emission. The Eu 3d XPS binding energies of SiO_2:$Eu^{2+}_{0.05}$ consist of 4 components, Eu^{2+} $3d_{5/2}$ (1126.1 eV), Eu^{3+} $3d_{5/2}$ (1135.8 eV), Eu^{2+} $3d_{3/2}$ (1155.9 eV), Eu^{3+} $3d_{3/2}$ (1165.4 eV). Considering the PL emission spectrum, it is evident that the Eu^{2+} ions in SiO_2:$Eu^{2+}_{0.05}$ compound is easily oxidized under X-ray irradiation. After thermal treatment of SiO_2:$Eu^{2+}_{0.05}$ compound under O_2 atmosphere at 1300℃ for 3h, the PL emission spectrum (bottom at right) was obtained. As its PL behavior shows the characteristic of Eu^{3+} with a line spectrum at 616 nm corresponding to the red emission, it is evident that the Eu^{2+} ions occupied into the SiO_2 matrix are nearly oxidized to Eu^{3+}. Thus, the Eu^{3+} 3d XPS spectrum (bottom at left) is predominantly obtained after thermal treatment of SiO_2:$Eu^{2+}_{0.05}$ compound under O_2 atmosphere at 1300℃ for 3h. From XPS measurement, the valuable information was obtained; the valence state of Eu ions occupied into the SiO_2 matrix is predominantly Eu^{2+}, associated

with the blue emission. However, XPS as a surface analysis technique, can't tell the total presence of Eu^{3+} in SiO_2: $Eu^{2+}_{0.05}$ compound even though there exists in small amount of Eu^{3+}. Thus, XPS results evidently imply that the Eu^{2+} ions stabilized in SiO_2 matrix are easily oxidized under X-ray irradiation in XPS measurements. ^{29}Si MAS-NMR spectra of SiO_2 compounds are given in Fig. 12. The chemical shifts for α-quartz (a) and α-cristobalite (b, after firing α-quartz fired at 1500℃ under 4% H_2/Ar) are -107.7 ppm and -109.3 ppm, respectively, which is in good agreement with those as previously reported.[37-39] α-quartz (a) and α-cristobalite (b) show essentially no "side-bands" and no "chemical shifts", indicating that there are neither different Si sites nor metal cations as shown in Fig 12. α-quartz is transformed into the mixed phase (c) with 10 wt% of α-quartz and 90 wt% of α-cristobalite after firing at 1300℃ under 4% H_2-Ar atmosphere, and the chemical shift of the mixed phase is -109.5 ppm which is similar to that of α-cristobalite. It is very notable that in SiO_2:Eu^{2+} compounds, "the spinning side-bands are appeared" depending on the Eu content; two weak side bands in SiO_2: $Eu^{2+}_{0.002}$ fired at 1500℃under 4% H_2-Ar (d) and SiO_2:$Eu^{2+}_{0.002}$ fired at 1300℃under 4% H_2-Ar (e), and six intense ones in SiO_2: $Eu^{2+}_{0.05}$ fired at 1300℃under 4% H_2-Ar (f). It is well-known that the spinning side-bands are originated from the dipolar interactions between the nuclear spin and the unpaired electron spins of the paramagnetic ions,[40-44] in this system between ^{29}Si spin and the unpaired electron spins of the Eu^{2+} ions. Thus, the fact that there are the spinning side-bands in MAS-NMR spectra of SiO_2:Eu^{2+} compounds, supports that the Eu^{2+} ions are occupied with a pseudo-covalent bond character in the interstitial sites of SiO_2 crystal lattice.

3.5 Hydrogen Assisted SiO_2-defects: Nano-SIMS Measurements.

It is well-known that the reducing atmosphere plays an important role in the controlling of oxygen vacancies as well as charge valences of metal ions in metal oxides. Certainly, this is the fact that the additional charges should be compensated in order to incorporate metal ions of lower valence into the interstitial sites as well as to replace Si^{4+} with metal ions of lower valence in SiO_2 matrix. The types of the point defect in silicon dioxide can be classified into intrinsic and extrinsic point defect. Intrinsic point defects involve vacancies caused by the missing host atoms and self-interstitials by additional host atoms at an interstitial position. Extrinsic point defects relate to foreign atom different from the host crystal. Defects in a perfect silicon dioxide could include O (or Si) vacancies, their interstitials, Si-Si (or O-O) homobonds, and under-coordinated silicons or oxygens.[45] Many authors considered hydrogen to be an intrinsic defect because it has been commonly found in silicon dioxide.[46-50] Mysovsky et al.[47] argued that the oxygen-deficient vacancy combined a hydrogen atom, E_4' center consists of a hydrogen substituting for an oxygen atom in α-quartz as the following reaction:

$$\equiv Si\text{-}O\text{-}Si\equiv + H \rightarrow \equiv Si\text{-}H + Si\equiv + O \text{ (interstitial)} \quad (1)$$

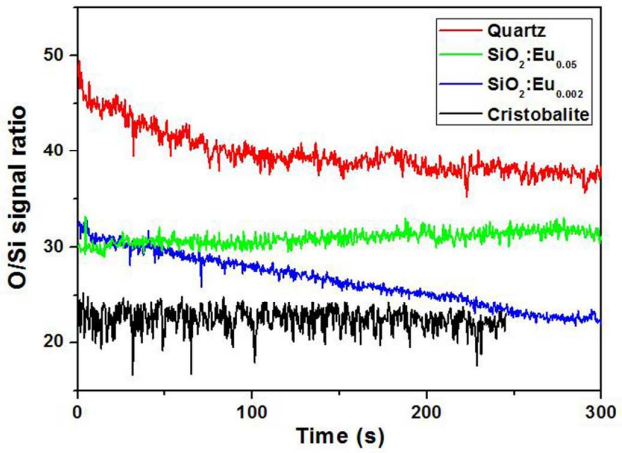

Fig. 13 O/Si signal ratios determined by TOF-SIMS depth profile in SiO_2-related compounds.

The neutral oxygen vacancy (ODC(|)) could be converted to ≡Si-O-H groups by thermal reaction with hydrogen molecules according to the following reaction:[51,52]

$$\equiv Si\text{-}Si\equiv + H_2 \rightarrow 2\{\equiv Si\text{-}O\text{-}H\} \quad (2)$$

The formation mechanism of hydrogenic trapped-hole species in α-quartz was proposed by Nuttall et al.,[48] which indicates that the hydrogen ions ($4H^+$) incorporated into α-quartz structure substitute for Si^{4+} as the following reaction:

$$4\{\equiv Si\text{-}O\}\text{-}Si(defect) + 4H^+ \rightarrow 4\{\equiv Si\text{-}O\text{-}H\} \quad (3)$$

The variation of the O/Si signal ratios of SiO_2 compounds is clearly seen depending on the firing condition as presented in Fig. 13. A sputtered depth profile of SiO_2 compounds obtained by time-of-flight secondary ion mass spectrometry (TOF-SIMS) corroborates the O-defective SiO_2 induced by hydrogen as discussed above. The O/Si signal ratio of α-quartz as received (Aldrich chemical) is the highest value, whereas those of SiO_2: $Eu^{2+}_{0.002}$ and SiO_2: $Eu^{2+}_{0.05}$ fired at 1300℃ under H_2 atmosphere are lower than that of commercially available α-quartz, indicating that the oxygen atoms are predominantly missing at high temperature under hydrogen atmosphere. Moreover, α-cristobalite obtained after firing α-quartz at 1500℃ under H_2 atmosphere shows the constant and lowest O/Si ratio. Although our Nano-SIMS analysis does not allow quantification of H content in the samples, the observed O/Si signal ratios are consistent with this formation mechanism.

3.6 Interstitial and Vacancy Mechanism of Eu^{2+} Doping in SiO_2 Matrix

The incorporation of Eu^{2+} ions into SiO_2 matrix may be explained in three different ways. **The first explanation** is that Eu atoms can replace silicon atoms forming a substitutional solid solution in a SiO_2 crystal. However, the direct substitution of Si^{4+} with Eu^{2+} is difficult because of the difference in the

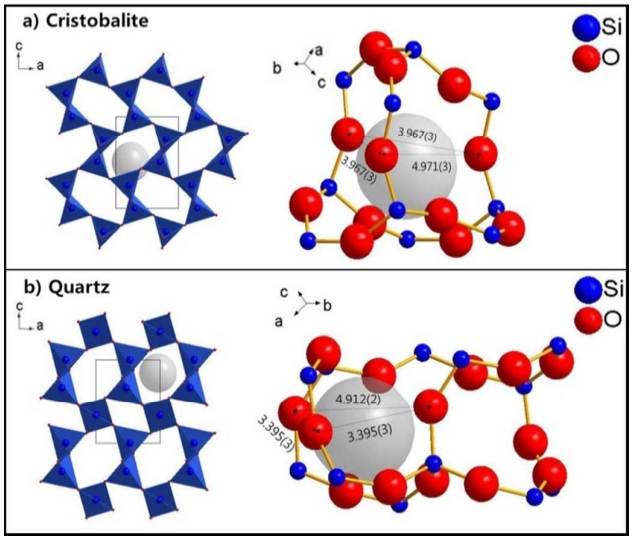

Fig. 14 The schematic representations of the crystal structures for α-cristobalite (top) and α-quartz (bottom). Si and O atoms are represented by blue and red spheres. Structural voids are represented by grey spheres with radius of 1.25 Å (Eu^{2+} at CN = 8).

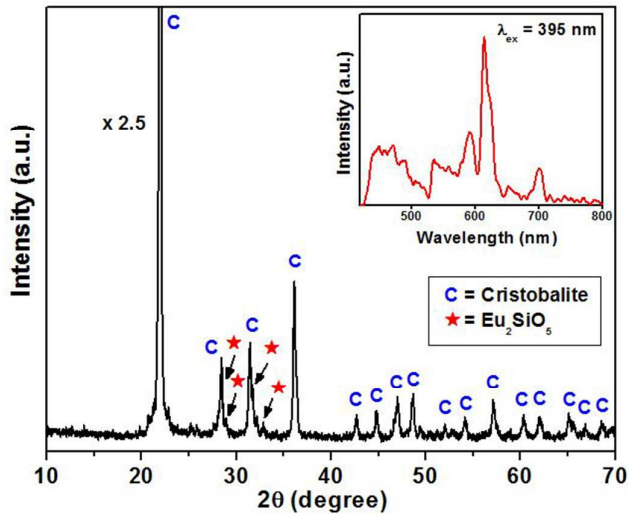

Fig. 15 XRD pattern of SiO_2:$Eu^{3+}_{0.01}$ fired at 1300℃ in O_2 atmosphere. The inset shows the PL emission spectra.

ionic radii of Si^{4+} (0.26 Å) and Eu^{2+} (1.30 Å).[53] Moreover, to best of our knowledge, there has been no report on the 4-coordinated Eu^{2+} (or. Eu^{3+}) in metal oxides as well as organometallic complexes. **As a second explanation**, the Eu atoms can distribute in the boundary of SiO_2 grains to form microscopic regions of europium oxide. The europium oxide can react with SiO_2 grains to generate Eu-containing silica compounds such as $EuSiO_3$ and Eu_2SiO_4. Several authors have reported the formation of $EuSiO_3$ and Eu_2SiO_4 on Eu-doped silica films in the studies.[54-56] Li et al. reported that Eu-doped SiO_2 films annealed in N_2 at temperature higher than 8 0 0 ℃ exhibited a broad emission band between 400 and 800 nm which was attributed to the formation of $EuSiO_3$ giving rise to intense yellow luminescence.[54] In Eu-doped SiO_2 films, the broad emission peak centered at 610 nm between 500 and 750 nm was observed due to the Eu^{2+} ions stabilized in the Eu_2SiO_4 and $EuSiO_3$ crystalline structures.[56] In our Eu^{2+}-doped SiO_2 compounds, the broad emission bands centered at 440 nm between 380 and 540 nm are observed indicating blue-emission. Moreover, Rietveld analyses within the Eu-doping range from 0.002 to 0.05 show that there is no trace of impurities which agree with the phase diagram of the EuO-SiO_2 system.[57] **As a third explanation**, we speculate that the Eu atoms can incorporate into the structural void spaces (interstitial sites). Both α-cristobalite and α-quartz have open structures as shown in Fig. 14. As the void spaces formed in α-cristobalite structure are somewhat larger than those in α-quartz structure, it is presumed that Eu^{2+} ions preferably occupy the interstitial sites of α-cristobalite. Compared with the ionic radius between Eu^{2+} (1.25 Å at C.N. = 8) and Eu^{3+} (1.066 Å at C.N. = 8),[53] Eu^{3+} ions are more favorable to the void spaces of SiO_2 matrix on condition that no other phases is formed in the EuO-SiO_2 solid-solution. However, in the Eu-doped SiO_2 compound fired at 1300℃ in air, the impurity phase of Eu_2SiO_5 (at the Eu-doping range of 0.01) is clearly observed in XRD pattern and this compound exhibited a faint reddish-emission attributed to the formation of Eu^{3+} ions as shown in Fig. 15, which indicates that in air atmosphere, Eu^{3+} ions cannot occupy the interstitial sites of SiO_2 matrix and but react with SiO_2 giving rise to the formation of Eu_2SiO_5 in air atmosphere within the Eu-doping ranges from 0.002 to 0.05. On the contrary, Eu^{2+} ions can enter the interstitial sites at 1300℃ under 4% H_2-Ar atmosphere. Thus, it is presumed that Eu^{2+} ions can be stabilized in the interstitial sites of SiO_2 matrix through the oxygen vacancies and partial fragmentation of tetrahedron linkages caused by hydrogen assistance. It should be noted that Eu_2O_3 (without adding SiO_2) was fired at 1300℃ under 4% H_2-Ar atmosphere and obtained a red-emitting Eu_2O_3 with a monoclinic structure. Based on the experimental results, Eu^{2+} doping mechanism in SiO_2 matrix could be postulated, as follows: ⅰ) the reduction of Eu_2O_3 (Eu^{3+}) to EuO (Eu^{2+}) at high temperature (≥1000℃) under hydrogen atmosphere, ⅱ) the entrance of Eu^{2+} ions in the interstitial sites of SiO_2 matrix through the oxygen vacancies and partial fragmentation of tetrahedron linkages caused by hydrogen assistance, ⅲ) the block of subsequent oxidation of the Eu^{2+} ions enclosed by Si-O linkages compared with the isolated Eu^{2+} species.

3.7 Theoretical Comparison of Interstitial Positions of Eu Atom in α-Cristobalite and α-Quartz: Interatomic Potential

We theoretically calculate the interatomic potentials depending on the interstitial positions of Eu atom in α-cristobalite and α-quartz, and compare their energy values. As shown in Fig. 16, α-cristobalite and α-quartz have large interstitial void spaces. When an Eu atom is located in the void spaces, the interatomic chemical forces between atoms exert. Atoms have strong repulsion forces when their distance is shorter than sum of their atomic radii. Ions have electric repulsion or attraction, depending on their charges.

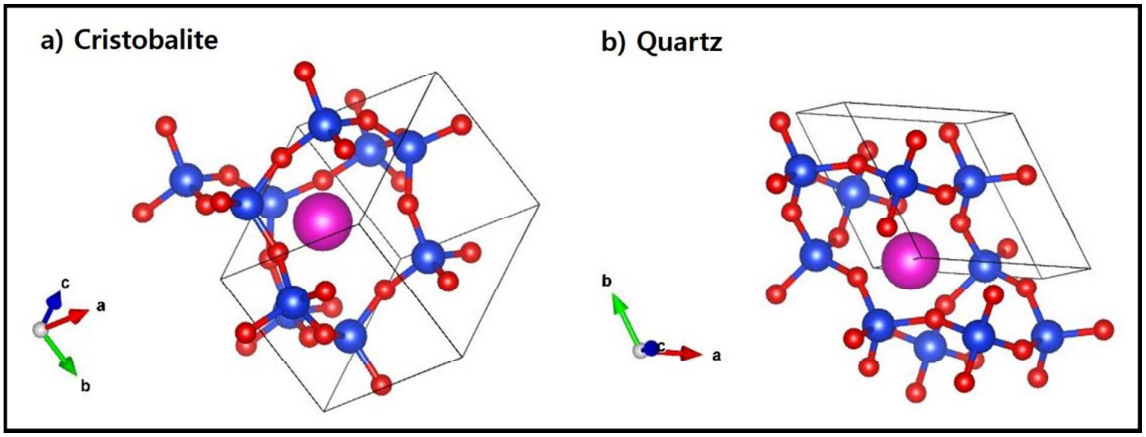

Fig. 16 . Eu^{2+} positions in the interstitial site of α-cristobalite (a) and α-quartz (b). Blue, red, purple dots are Si, O, Eu atoms respectively.

The former can be modeled by Lennard-Jones potential[58] and the latter can be modeled by coulomb potential.[58] The potential can be written as

$$U(\vec{r}) = \sum_i \varepsilon_i \left(\left(\frac{r_i}{|\vec{r} - \vec{R}_i|} \right)^{12} - 2 \left(\frac{r_i}{|\vec{r} - \vec{R}_i|} \right)^{6} \right) + \sum_i k_e \frac{Z_{Eu} Z_i e^2}{|\vec{r} - \vec{R}_i|}, \quad (4)$$

where first sum is the Lennard-Jones potential of nearby ions and second sum is the coulomb potential. Index i is related to the surrounding atoms in the crystal (ε_i : bond dissociation energy, $\vec{R}_i$: the location of i^{th} atom, r_i : the minimum potential distance between Eu^{2+} and i^{th} atom, Z_{Eu}: charge number of Eu^{2+}, Z_i : charge number of i^{th} atom). There are two kinds of atoms around Eu, O and Si. For O, we choose ε_i as Eu-O bond dissociation energy 473 KJ/mol = 4.903 eV.[59] r_i is chosen as sum of ionic radius of Eu^{2+} (1.30 Å) and crystal radius O^{2-} (1.34 Å), Z_i for O charge number is -1 from consideration of half ionic character. For Si, it does not form a bond with Eu^{2+} ions. We choose r_i as sum of ionic radius of Eu^{2+} (1.30 Å) and crystal radius of Si (0.26 Å) and determine value ε_i as 4.892 eV which gives same repulsion force as Eu and O Lennard-Jones force when atomic distance is compressed to 80% of their sum of radii. Z_i for Si charge number is 4, O charge number -2 and Z_{Eu} is 2. The local minimum point of this potential in three dimension can be found numerically, by successively following the negative gradient of potential (force) which gives steepest descent. Starting from initial position, search next potential minimum in finite interval of force direction, and repeat the procedure until it converges. In α-cristobalite case, the minimum position is shown in Fig. 16. Crystal unit cell parameters are given by (a, b, c) = (4.978, 4.978, 6.948) (Å), (α, β, γ) = (90, 90, 120) (°degree) and Eu minimum position is (0.26758, 0.25590, 0.50357) in unit cell coordinate. Nearby oxygen coordinates are (0.1032, 0.2397, 0.8216), (0.7397, 0.3968, 0.5716), (0.2397, 0.1032, 0.1784), (0.3968, 0.7397, 0.4284). Their distances from Eu atom are Their distances from Eu are 2.504, 4.325, 2.769, 4.293 Å. Thus, the calculated minimum potential value is -51.47 eV. In α-quartz case, the minimum position is shown in Figure 16. Crystal unit cell parameters are given by (a, b, c) = (4.912, 4.912, 5.404) (Å), (α, β, γ) = (90, 90, 120) (°degree) and Eu minimum position is (-0.0301, 0.0014, 0.6674) in unit cell coordinate. Nearby oxygen coordinates are (0.4136, 0.2676, 0.7857), (0.1460, -0.2676, 0.5476), (-0.4136, -0.1460, 0.8801), (-0.2676, 0.1460, 0.4524). Their distances from Eu are 2.005, 2.014, 2.008, 2.011 Å. Minimum potential value is calculated to be 221.8 eV. The results suggest that it is more difficult to put Eu atom into α-quartz than α-cristobalite. In α-cristobalite case, minimum potential is negative as well as the distances between atoms at minimum point are large. Only two oxygens around 2.5 and 2.7 Å and next nearest oxygen distances are larger than 4 Å. In α-quartz case potential value is positive, which implies instability. Also the nearby oxygen distances are almost identically 2 Å at minimum potential point, showing quite regular and closely packed structure. It is reasonable to infer that Interstitial positioning of Eu is more easily done in α-cristobalite case than α-quartz case.

4 Conclusions

Blue-emitting silica by Eu^{2+}-activator ion occupied in the interstitial sites of SiO_2 matrix, has been successfully synthesized and characterized. The PL excitation spectra of SiO_2:$Eu_{0.01}$ compounds monitored at 438 nm, consist of broad bands between 220 nm and 420 nm, which may be ascribed to the allowed $4f^7$– $4f^6$5d transitions of Eu^{2+}, which is in good agreement with XPS results. The emission spectra monitored under the 323 nm excitation, show symmetric bands centered around 438 nm, which is associated with blue-emission. From FT-IR spectra of SiO_2 compounds with and without Eu^{2+}-activator ions, it clearly shows that the lower absorbance and greater broadness are observed in the IR modes of SiO_2:Eu^{2+} compounds compared with those of α-quartz and α-cristobalite without Eu^{2+}-activator ions, indicating that the Eu^{2+}-activator ions are well located in the interstitial sites of SiO_2 matrix with a pseudo-covalent bond character between Eu ion and O ion sharing with SiO_4 tetrahedral units. ^{29}Si MAS-

NMR spectra corroborates the interpretation of IR results. The fact that there are the spinning side-bands in MAS-NMR spectra of SiO_2:Eu^{2+} compounds, supports that the Eu^{2+} ions are occupied with a pseudo-covalent bond character in the interstitial sites of SiO_2 crystal lattice. The interatomic potentials depending on the interstitial positions of Eu atom in α-cristobalite and α-quartz are calculated using Lennard-Jones potential and coulomb potential; for α-cristobalite the minimum potential value is -51.47 eV, for α-quartz 221.8 eV, which reveals that the Eu^{2+}-activator ions more preferably enter the interstitial sites of α-cristobalite than those of α-quartz. Thanks to the Eu^{2+}-activator ions occupied in the SiO_2 matrix, the PL intensity of SiO_2:$Eu^{2+}_{0.002}$compound is about 24 times as high as that of the O-defective SiO_2 compound and the relative emission intensity of SiO_2:$Eu^{2+}_{0.002}$ monitored at 300 nm is about 40% compared to a commercial BAM:Eu^{2+} (obtained from Nichia Co. Ltd. in Japan). This phosphor material could be a breakthrough for modeling a new phosphor and application in the solid state lighting field.

Acknowledgements

This research was financially supported by the Ministry of Education (MOE) and National Research Foundation of Korea (NRF) through the Human Resource Training Project for Regional Innovation (2014H1C1A1066859). One of the authors, S. J. Kim, acknowledges support from the National Research Foundation (NRF) of Korea (Grant No. 2009-0094046). Dr. Seen Ae Chae at the KBSI is acknowledged for carrying out NMR experiments. We would like to thank NSFs Major Research Instrumentation (NSFARRA award #0960334) and Arizona State University for acquisition and installation of the Nano-SIMS 50L.

References

1 N. N. Greenwood and A. Earnshaw, *Chemistry of the Elements*, Pergamon Press: Oxford, 1984.
2 A. F. Wells, *Structural Inorganic Chemistry*, Clarendon Press: Oxford, 1984**.**
3 IARC. *IARC Monogr Eval Carcinog Risks Hum.,* 1997, **68**, 1, PMID:9303953.
4 M. E. Zolensky, P. J. Sylvester and J. B. Paces, *American Mineralogist*, 1988, **73**, 313-323.
5 G. Dantelle, M. Mortier, D. Vivien and G. Patriarche, *Chem. Mater*., 2005, **17**, 2216-2222.
6 S. Sivakumar, F. C. J. M. van Veggel and M. Raudsepp, *J. Am. Chem. Soc.,* 2005, **127**, 12464-12465.
7 D. Starick, S. I. Golovkova and A. M. Gurvic, *J. Lumin*., 1988, **40&41***,* 199-200.
8 F. E. Swindells, *J .Electrochem. Soc.,* 1954, **101**, 415-418.
9 R. Stefani, A. D. Maia, E. E. S. Teotonio, M. A. F. Monteiro, M. C. F. C. Felinto, and H. F. Brito, *J. Solid State Chem.,* 2006**, 179**, 1086-1092.
10 X. Piao, T. Horikawa, H. Hanzawa and K. Machida, *Appl. Phys. Lett.,* 2006, **88**, 161908-161913.
11 W. B. Im, Y. K. Kim and D. Y. Jeon, *Chem. Mater.,* 2006, **18**, 1190-1195.
12 D. P. Yu, Q. L. Hang, Y. Ding, H. Z. Zhang, Z. G. Bai, J. J. Wang, Y. H. Zou, W. Qian, G. C. Xiong and S. Q. Feng, *Appl. Phys. Lett*., 1998, **73**, 3076-3078.
13 L. D. Carlos, V. de Zea. Bermudez, R. A. Sa´ Ferreira, L. Marques and M. M. Assunçâo, *Chem. Mater*., 1999, **11**, 581-588.
14 T. Uchino, N. Kurumoto and N. Sagawa, *Phys. Rev. B.*, 2006, **73**, 233203-233206.
15 A. Aboshi, N. Kurumoto, T. Yamada and T. Uchino, *J. Phys. Chem. C,* 2007, **111**, 8483-8488.
16 S. Banerjee and A. Datta, *Langmuir*, 2010, **26**, 1172-1176.
17 S. Yang, W. Li, B. Cao, H. Zeng and W. Cai, *J. Phys. Chem. C,* 2011, ***115***, 21056-21062.
18 J. M. McCrate and J. G. Ekerdt, *Chem. Mater*., 2014, **26**, 2166-2171.
19 T. C. Liu, H. Kominami, H. F. Greer, W. Zhou, Y. Nakanishi and R. S. Liu, *Chem. Mater*., 2012, **24**, 3486-3492.
20 J. Rodriguez-Carvajal, *Fullprof 2000: A Rietveld Refinement and Pattern Matching Analysis Program, April* 2008*, Laboratoire Léon Brillouin (CEA-CNRS)*.
21 S. Zhang, Y. Nakai, T. Tsuboi, Y. Huang and H. J. Seo, *Chem. Mater*., 2011, **23**, 1216-1224.
22 W. B. Im, Y. I. Kim, H. S. Yoo and D. Y. Jeon, *Inorg. Chem*., 2009, **48**, 557-564.
23 K. Inoue, N. Hirosaki, R. J. Xie and T. Takeda, *J. Phys. Chem.* C, 2009, **113***,* 9392-9397.
24 J. Hlavay, K. Jonas, S. Elek and J. Inczedy, *Clays Clay Miner*., 1978, **26**, 139-143.
25 A. M. Pires and M. R. Davolos, *Chem. Mater*., 2001, **13**, 21-27.
26 D. Kim, D. Park, N. Oh, J. Kim, E. D. Jeong, S. J. Kim, S. Kim, J. C. Park, *Inorg. Chem*., 2015, **54**, 1325-1336.
27 R. C. Weast, Handbook of Chemistry and Physics, CRC Press, 1990.
28 L. Li, G. Li, Y. Che and W. Su, *Chem. Mater*., 2000, **12**, 2567-2574.
29 S. Fujihara and K. Tokumo, *Chem. Mater*., 2005, **17**, 5587-5593.
30 Y. P. Du, Y. W. Zhang, L. D. Sun and C. H. Yan, *J. Phys. Chem. C,* 2008, **112**, 12234-12241.
31 E. J. Cho and S. J. Oh, J. *Phys. Rev. B*., 1999, **59**, R15 613-616.
32 J. Qi, T. Matsumoto, M. Tanaka and Y. Masumoto, *J. Phys. D: Appl. Phys*., 2000, **33**, 2074-2078.
33 L. Cario, P. Palvadeau, A. Lafond, C. Deudon, Y. Moëlo, B. Corraze and A. Meerschaut, *Chem. Mater*., 2003, **15**, 943-950.
34 D. Y. Lu, M. Sugano, X. Y. Sun and W. H. Su, *Appl. Surf. Sci*., 2005, **242**, 318-325.
35 C. Caspers, M. Müller, A. X. Gray, A. M. Kaiser, A. Gloskovskii, C. S. Fadley, W. Drube and C. M. Schneider, *Phys. Status Solidi RRL*., 2011, **5**, 441-443.
36 W. Jiang, Z. Bian, C. Hong and C. Huang, *Inorg. Chem*., 2011, **50**, 6862-6864.
37 E. Lippmaa, M. Mägi, G. Engelhardt and A. R. Grimmer, *J. Am. Chem. Soc*., 1980, **102**, 4889-4893.
38 J. V. Smith and C. S. Blackwell, *Nature*, 1983, **303**, 223-225.
39 K. A. Smith, R. J. Kirkpatrick, E. Oldfield and D. M. Henderson, *Am. Mineral*., 1983, **68**, 1206-1215.
40 W. Huang, M. Schopfer, C. Zhang, R. C. Howell, L. Todaro, B. A. Gee, L. C. Francesconi and T**.** Polenova, *J. Am. Chem. Soc*., 2008, **130**, 481-490.
41 S. L. Poulsen, V. Kocaba, G. L. Saoût, H. J. Jakobsen, K. L. Scrivener and J. Skibsted, *Solid State Nucl. Magn. Reson.,* 2009,**36**, 32-44.
42 S. Ivanova, E. Zhecheva, R. Stoyanova, D. Nihtianova, S. Wegner, P. Tzvetkova and S. Simova, *J. Phys. Chem. C,* 2011, **115**, 25170-25182.
43 A. Ferreira, D. Ananias, L. D. Carlos, C. M. Morais and J. Rocha, *J. Am. Chem. Soc*., 2003, **125**, 14573-14579.
44 M. B. Ley, D. B. Ravnsbæk, Y. Filinchuk, Y. S. Lee, R. Janot, Y. W. Cho, J. Skibsted and T. R. Jensen, *Chem. Mater.,* 2012, **24**, 1654-1663.

45 S. Basu, *Crystalline Silicon-Properties and Uses*, InTech, 2011.
46 R. A. Weeks, *Phys. Rev*., 1963, **130**, 570-576.
47 A. S. Mysovsky, P. V. Sushko, S. Mukhopadhyay, A. H. Edwards and A. L. Shluger, *Phys. Rev. B.*, 2004, **69**, 85202.
48 R. H. D. Nuttall and J. A Weil, *Solid State Commun*., 1980, **33**, 99-102.
49 A. C. McLaren, R. F. Cook, S. T. Hyde and R. C. Tobin, *Phys. Chem. Minerals*, 1983, **9**, 79-94.
50 P. E. Blöchl and J. H. Stathis, *Phys. Rev. Lett*., 1999, **83**, 372-375.
51 H. Imai, K. Arai, H. Imagawa, H. Hosono and Y. Abe, *Phys. Rev. B.*, 1988, **38**, 12772-12775.
52 H. Hosono, Y. Abe, H. Imagawa, H. Imai and K. Arai, *Phys. Rev. B.*, 1991, **44**, 12043-12045.
53 R. D. Shannon, *Acta Crystallogr*., 1976, **32**, 751-767.
54 D. Li, X. Zhang, L. Jin and D. Yang, *Optics Express,* 2010, **18**, 27191-27196.
55 J. Qi, T. Matsumoto, M. Tanaka and Y. Masumoto, *Electrochem. Solid-State Lett.,* 2000, **3**, 239-241.
56 L. Li, J. Zheng, Y. Zuo, B. Cheng and Q. Wang, *Nanoscale Res Lett.,* 2013, **8**, 194.
57 M. W. Shafer, *J. Appl. Phys.,* 1965**, 36**, 1145-1151.
58 P. Atkins, J. Paula, *Physical Cehmistry*, 8th edition, Oxford University Press, 2006.
59 Y. Luo, *Comprehensive handbook of chemical bonding energies*, CRC Press, 2007.